Available online at www.sciencedirect.com

ScienceDirect

Ceramics International 40 (2014) 3925–3931

CERAMICS INTERNATIONAL

www.elsevier.com/locate/ceramint

Effect of the solid precursors on the formation of nanosized TiB_x powders in RF thermal plasma

Szilvia Klébert[a,*], Anna Mária Keszler[a], István Sajó[a], Eszter Drotár[a], Imre Bertóti[a], Eszter Bódis[a], Péter Fazekas[a], Zoltán Károly[a], János Szépvölgyi[a,b]

[a]Institute of Materials and Environmental Chemistry, Research Centre for Natural Sciences, Hungarian Academy of Science, Budapest, Hungary
[b]Research Institute of Chemical and Process Engineering, University of Pannonia, Veszprém, Hungary

Received 11 July 2013; received in revised form 31 July 2013; accepted 7 August 2013
Available online 15 August 2013

Abstract

Continuous synthesis of TiB_x ($x \approx 0.5$–2) nanoparticles from various low cost solid precursors such as titanium and titanium dioxide admixed with boron and/or carbon in radiofrequency thermal plasma was studied. Feasibility of TiB_2 formation was predicted by thermodynamic equilibrium calculations in the 500–5000 K temperature range. In all the investigated system high temperature reactions resulted in nanometer-sized TiB_x powders with a mean size varying between 13 and 83 nm. The yield of particular runs ranged from 38% to 97%. Among the synthesized products in addition to TiB_x, oxidized precursor residues were also found in smaller quantities. Although addition of carbon to the precursors could not completely prevent surface oxidation of boride particles, it contributed to the reduction of the mean particle size of the formed TiB_2.

Keywords: A. Powders: chemical preparation; A. Powders: gas phase reaction; D. Borides; A. RF plasma synthesis

1. Introduction

Titanium diboride (TiB_2) is a non-oxide refractory ceramic material with excellent properties such as high melting point (3225 °C), high hardness (25–35 GPa), high thermal (60–120 W/(m K)) and electrical conductivity ($\sim 10^5$ S/cm), resistance to mechanical erosion and chemical corrosion. This combination of properties makes TiB_2 a candidate for high performance applications including wear resistant parts, metal melting crucibles, composite and electrode materials [1,2]. Recently, interest in high-melting compounds has increased in connection with nanostructural materials [3]. Nanoparticulate titanium diboride is also of particular interest among refractory compounds [4].

A variety of methods are known for TiB_2 powder synthesis. Currently, mass production is based on the carbothermic/borothermic reduction of titanium oxide with boron carbide. This process, however, resulted in mainly micronsized particles. Processes for nanopowder synthesis such as self-propagating high temperature synthesis (SHS) [5], vapor-phase synthesis [3,6,7], the carbothermal reduction process [1] and high energy ball milling [8] have also been developed. All the mentioned processes have their merits and limitations over the others such as the cheaper precursors they use or the lower reaction temperature, the higher purity of the obtained product, smaller particle size, etc. It is beyond the scope of this article to make detailed comparison of these processes and judge them in terms of feasibility. Instead, in the present article the authors report on a thermal plasma process also for the synthesis of nanometer-sized SiC powder, which combines the benefits of low cost precursors with continuous processing.

By virtue of its unique combination of properties the Radio-Frequency (RF) thermal plasma process offers a convenient route for preparing nanosized particles either in metallic or ceramic systems [9–16]. Thermal plasmas have been mainly utilized in such processes, where the extremely high temperature that can reach several thousand degrees provides advantage to establish a more economical processing route [17–22]. In addition, it makes possible a continuous process and the ease of scaling up [23,24]. The main question is whether or not the residence times of solid precursors in the plasma enough

*Corresponding author. Fax: +36 1 438 1147.
E-mail address: klebert.szilvia@ttk.mta.hu (S. Klébert).

0272-8842/$ - see front matter © 2013 Elsevier Ltd and Techna Group S.r.l. All rights reserved.
http://dx.doi.org/10.1016/j.ceramint.2013.08.036

for an in-flight reaction. Although theoretical calculations showed that titanium particles under a critical size can evaporate in the plasma, these calculations usually relates single particle loading and not under dense loading conditions when simultaneous feeding of a mixture of different types of particles occurs [25]. Among the very few papers dealing with experimental plasma synthesis of TiB_2, Cheng at al. [7] studied the formation mechanism of titanium boride starting from Ti and B powders with varying ratio. Their findings were that feed rate of precursors and boron content affect the crystalline size of the final product and that the residence time was insufficient for full evaporation of the precursors.

In respect of residence time RF plasma has an advantage over arc plasma due to the more extended plasma flames that result in longer mean residence time of reactive species in the hot plasma region [26].

In this work the synthesis of nanosized TiB_x powders from low cost materials in RF thermal plasma were studied. We investigated the feasibility of an in-flight reaction when reactants are fed in solid form and compared the different systems in terms of efficiency of the reduction and morphology of the resulted products.

2. Material and methods

In the experiments thermal plasma processing of four different material systems was investigated: (1) Processing (evaporation) of micrometer sized TiB_2 (Grade D, ABCR GmbH & Co KG, 1–7 μm) to condense nanometer-sized powder. (2) Mixture of micron-sized titanium (Alfa Aesar, 45micron, 99%) and boron (ABCR GmbH & Co KG, 98%) powders in different proportions. (3) Mixture of TiO_2 (Aldrich, 45micron, 99%) and B. Finally, (4) Carbon powder (graphite KS4, Timcal Co., $D_{50}=2.8$ μm) was also added to the feeding mixture of TiO_2 and B to create reducing atmosphere during synthesis.

Thermal plasma processing was performed in a RF plasma system using a 3–5 MHz, TEKNA PL-35 torch. The experimental set-up is described elsewhere [26]. The powders were injected axially into the hottest zone of the plasma flame by a PRAXAIR powder feeder.

Experimental conditions of the plasma treatments were as follows: feeding rate of the solid precursors was 3 g min^{-1}, while the input RF power varied between 0.5 and 0.75 kWh g^{-1}. The flow rate of He carrier gas was of 9 l min^{-1}, while the plasma gas consisted of Ar (15 l min^{-1}) and He (6 l min^{-1}). The sheath gas mixture composed of Ar and He in 30 to 19 l min^{-1} ratio. The argon and the helium were of 4.6 purity. Selection of working parameters was based on tests for the synthesis of nanoparticles using the same technique [9–13,27]. Helium was added both to the plasma and the carrier gas because of its high thermal conductivity and enthalpy, compared to other inert gases [11].

XRD patterns were obtained with a Philips instrument PW 3710 equipped with a PW 1050 Bragg–Brentano parafocusing goniometer, using monochromatized Cu Ka radiation. The XRD scans were digitally recorded with steps of 0.04° in the 2 h range from 4° to 80°. Quantitative phase composition was evaluated using a full profile fit method with corrections for preferred orientation and micro absorption [28]. The specific surface area was measured by nitrogen adsorption at 77 K and evaluated on the basis of BET isotherms (Quantachrome, Autosorb-1, seven point isotherm). The average particle size of synthetized powders was calculated by the following relation: $SSA=6/\rho d$, where ρ is the particle absolute density ($cm^3\ g^{-1}$), d is the diameter (μm) of the spherical particles and SSA is the measured specific surface area ($m^2\ g^{-1}$).

The morphology of synthesized powders was characterized by scanning electron microscopy (SEM, Zeiss type DSM 982 GEMINI with a heated field emission tungsten cathode) and transmission electron microscopy (TEM, Morgagni 268D). The surface chemical composition was studied by XPS (Kratos XSAM 800). Chemical states of the constituent elements and impurities were identified and assigned by available reference data bases and publications [29,30].

3. Results and discussion

3.1. Thermodynamic calculations

In thermal plasmas complete or partial evaporation and dissociation of the solid precursors may occur. Dissociated precursors recombine to form various products which will be nucleated from a supersaturated vapor phase. Short residence time of the reagents in the hot regions might not allow achieving the chemical composition corresponding to thermal equilibrium conditions. Yet, thermodynamic calculations based on the minimization of the system total free energy can provide suitable data for potential products and their concentrations [31]. In order to predict the plasma synthesis results we have carried out thermodynamic equilibrium calculations with the FACTSAGE [32] software in the 500–7500 K temperature range. Calculations were performed for the Ti+2B and TiO_2+4B, and also for the TiO_2+3B+3C systems.

In the equilibrium composition of Ti+2B system (which is analogous with introducing TiB_2) for temperature above 4000 K the main species in the gas phase are atomic Ti, atomic B and B_2 molecules. Formation of TiB_2 is favored over wide temperature range from 500 to 2900 K as solid and from 2900 to 3800 K as liquid.

In the case of TiO_2+4B system the equilibrium gas-phase composition is more complex, containing additionally BO(g) above 2500 K, as well as Ti(g), TiO(g) and O(g) above 3500 K (Fig. 1.). The condensed phase below 2000 K comprises only TiB_2, B and B_2O_3.

The goal of carbon addition to precursor materials is to remove the oxygen from the system in the form of CO instead of B_2O_3. Indeed, the presence of carbon leads to the formation of CO(g), although at higher temperatures C(g), C_2(g) and BC (g) appear, too. As a result the O(g) and BO(g) content remains negligible up to 5000 K. Below 3500 K the condensed state contains mainly TiB_2(s), while below 1500 K C(s), TiC(s) and some amount of B_2O_3(l) are also present among the products. Although condensed phase of B_4C seems to be stable only in the temperature range of 2000 K to 2500 K, its appearance

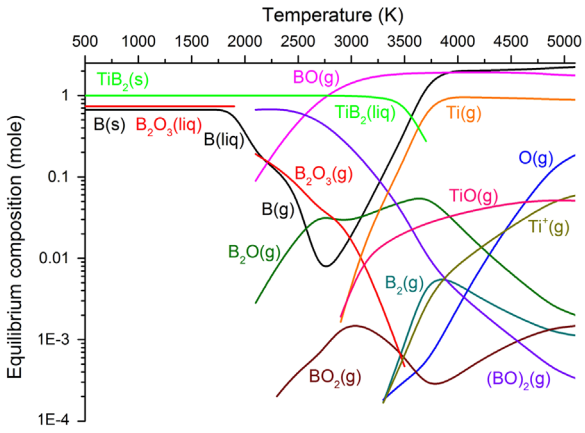

Fig. 1. Chemical equilibrium diagram for the TiO_2+4B system.

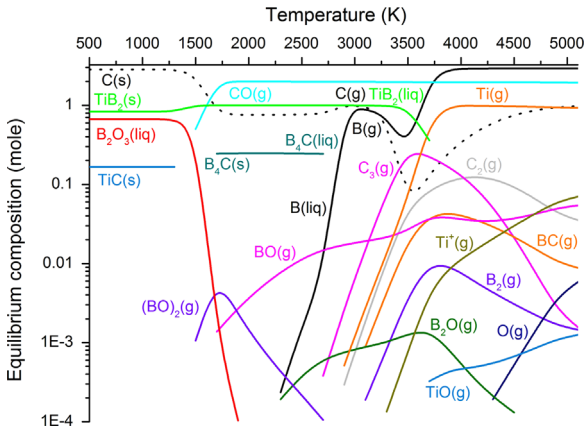

Fig. 2. Chemical equilibrium diagram for the $TiO_2+3B+3C$ system.

among product particles cannot be excluded. This is because that in plasma conditions the first condensed phase cannot react further due to the high cooling rates. Hence, thermodynamically non-equilibrium phases can be frozen even at lower temperatures [33,34] (Fig. 2.).

3.2. Powder characterization

In Table 1, the semi-quantitative composition based on the XRD intensities [35], specific surface area values and the calculated particle size of the prepared powders are presented.

3.3. Crystallographic phase relations

XRD analysis of product powders clearly confirms the formation of TiB_2 and TiB in all tests, although in rather different quantities. The formation of TiB_2 in Run 1 in remarkably high amount is not of a great surprise. The nanometer ranged size of the obtained particles, however, suggests that these particles formed from the vapor phase after evaporation of the solid particles in the plasma flame. The residence time of the formed particles in the high temperature zone was not sufficient for further growing. The small amount of oxide phase indicates that oxygen contamination was also present in the airtight system. It is worth noting that for the $Ti+B$ and also for the TiO_2+B system the set XRD peaks characteristic for α-titanium was detected in unexpectedly large quantity. These peaks could be fitted, however, with significantly increased lattice parameters, $a_0=2.957$ Å and $c_0=4.705$ Å, as compared to those measured for the fed Ti powder precursor, with $a_0=2.905$ Å and $c_0=4.6826$ Å. These latter lattice parameters are also characteristics for bulk titanium [36]. Accordingly, the increased lattice parameters suggests a phase (indicated as Ti(B)), in which boron is dissolved in the titanium lattice, but its concentration was less than that of the known TiB phase. Similar diffusions (hydrogen, carbon and boron) in a metal lattice were observed earlier. Mobility of hydrogen in metal lattices is a greatly investigated subject [37]. Due to the relatively small size of boron it also easily diffuses into a variety of metals, including ferrous, nickel and cobalt alloys [38,39]. In Run 2, beyond these phases TiB was also detected as an orthorhombic phase. The significantly lower amount of TiB_2 in Run 2 as compared to Run 1 suggests that part of the fed boron was reacted with the always present oxygen contaminants, even though such phase could not be detected among the crystal phases.

In Run 3, when TiO_2+4B mixture was injected into the plasma TiB_2 was the dominating phase among the product particles. Here again the boron doped titanium phase appeared, while smaller amount of Ti can be also detected in a Ti_2O_3 form, although it was not predicted by thermodynamic calculation. These facts suggest that the added boron was not sufficient to take up all the oxide and to form diboride with titanium. It was also experienced in earlier works [9] that stochiometric ratio in the feedstock composition usually does not result in complete reaction in practice. Significant amount of boron was oxidized and distinguished by XRD as H_3BO_3. Presence of B_2O_3 was anticipated in the final solid composition by thermodynamic calculation as a by-product combining the introduced oxygen. The formation of the detected H_3BO_3 phase could be attributed to the reaction of the formed B_2O_3 with water vapor that could be present in the reactor as contamination of the plasma gases. Anyway the H_3BO_3 can be easily washed out from the product. The small amount of Ti_2O_3 that was not predicted by thermodynamic calculation either may be formed from both TiB_2 and Ti(B), reacting with the O_2 contamination of the plasma gases at elevated temperature.

In the case of $TiO_2+3B+3C$ system (Run 4) the synthetized powder mixture contains, in addition to TiB_2, a large amount of B_4C (Fig. 3). A significant quantity of TiC was also detected in this sample with the lattice parameter of 4.28 Å. This value is between the reference one for TiC ($a_0=4.327$ Å) and for cubic TiO ($a_0=4.185$ Å) referring to a solid solution of the above two phases. Oxidized titanium was found both as Ti_2O_3 and TiO, while oxidized boron was detected (again as H_3BO_3) only in negligible quantity. These findings seemingly contradict the results of thermodynamic calculations, which predicted the formation of B_2O_3 as the only oxygen-containing solid phase, bounding all the oxygen fed in the form of TiO_2. The presence of carbon, detected as graphite, however, was also expected in the equilibrium product by thermodynamic calculations. Since B_4C, Ti_2O_3 and TiO should not be among

Table 1
Precursors and characteristics of the as-prepared powders.

Run	Precursors molar ratio	Composition of the synthesized powders (wt%) by XRD						SSA ($m^2\ g^{-1}$)	d_{BET} (nm)
		TiB_2	Ti(B)/TiB	B_4C/TiC	H_3BO_3	Ti_2O_3/TiO	C		
1	TiB_2	97	–	–	–	3/0	–	29	45
2	Ti+2B	54	40/6	–	–	–	–	21	63
3	TiO_2+4B	55	11/0	–	25	9/0	–	16	83
4	TiO_2+3B+3C	38	–	22/5	d*	18/5	12	101	13

*Detected in negligible quantity.

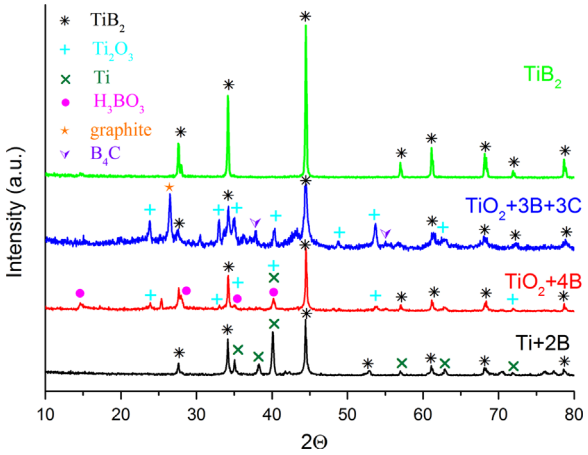

Fig. 3. XRD patterns of the products of particular Runs.

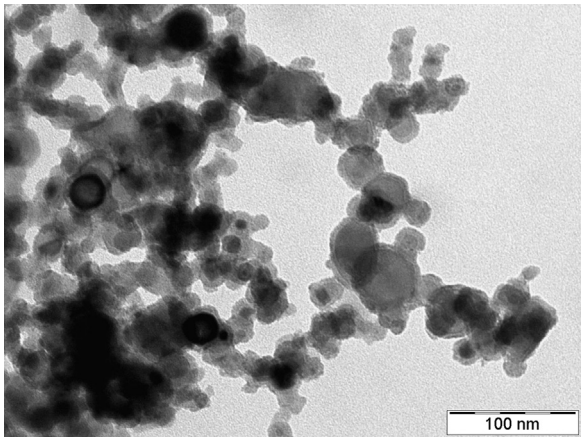

Fig. 4. TEM micrograph of TiB_2.

the equilibrium phases at room temperature, their presence in the product powder points out the significant role of kinetics of phase formation in the temperature range of 1500–3000 K following the rapid quenching of the product, thus preserving these detected non-equilibrium phases. In addition, it seems that carbon addition for reduction of TiO_2 was a questionable choice as boron also has a great tendency to form carbide and in this way not enough boron was left to react with Ti to form TiB_2. We suggest this was the reason for the lowest titanium-boride yield among the various Runs. Due to boron carbide formation the carbon was also not sufficient for the complete reduction of all the TiO_2.

3.4. Particle morphology

Mean size of TiB_2 particles were calculated from the values of the specific surface areas (SSA) of the product powders assuming spherical shape (Table 1). The SSA varied in the particular Runs within the range of 20–100 m^2g^{-1}. Accordingly the mean size could be estimated to fall between 13 nm and 83 nm. Although the assumption for sphericity may not completely be satisfied, the obtained results are in accordance with TEM analysis (Figs. 4–7). The nanoscale of the product particles is another consequence of the fast cooling process conditions characteristics for the plasma. The particles that nucleate from the vapor phase get out from the high temperature zone rapidly (within a few msec) and deposit on the reactor wall or flow away to the much cooler powder separator unit where further growing is hindered. In this way nanoparticles with nonequilibrium phases can also be formed [33,34]. In Run 1 TiB_2 nanoparticles with mean particle size of 40–50 nm are formed from the gas phase by condensation after the complete evaporation of the fed 1–7 μm-size precursor powder. TEM micrograph (Fig. 4) of the product particles of Run 1 is in agreement with SSA calculations as it shows relatively homogeneous distribution of particles with 30–80 nm size. This also confirms that evaporation and subsequent crystallization of the TiB_2 must take place from the gas phase.

Similar agreement of the mean particle size for Run 2 and the TEM micrographs (Fig. 5) taken of the products was established.

Prior to TEM investigation of Run $3H_3BO_3$ content was removed by water. The size of particles shows a significant heterodispersity in the range of 20–80 nm. In accordance with the XRD results two different phases can be distinguished for this sample: the more transparent crystals that could be assigned to the TiB_2 phase, while the darker ones to the Ti(B) phase. This assignment is consistent with their measured relative proportion determined by XRD, and with the known fact of higher absorptivity of electrons of that crystallites containing higher concentration of Ti. According to the micrograph the TiB_2 phase looks plate like while the Ti rich phase may be rather equiaxed and more faceted (Fig. 6).

The smallest mean particle size, 13 nm, was achieved when carbon was also added to the mixture of TiO_2 and B (Run 4, Table 1.). TEM micrographs (Fig. 7) of the powders of Run 4

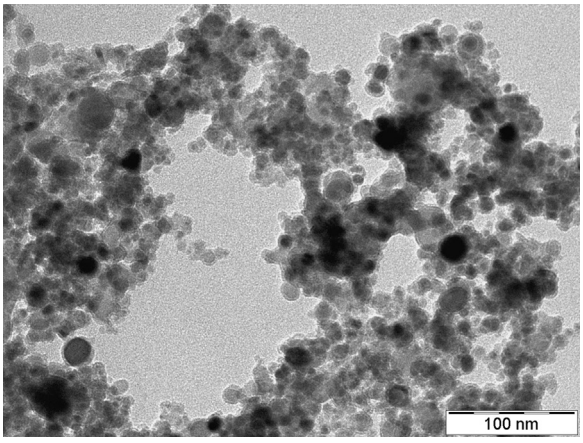

Fig. 5. TEM micrograph of Ti+2B.

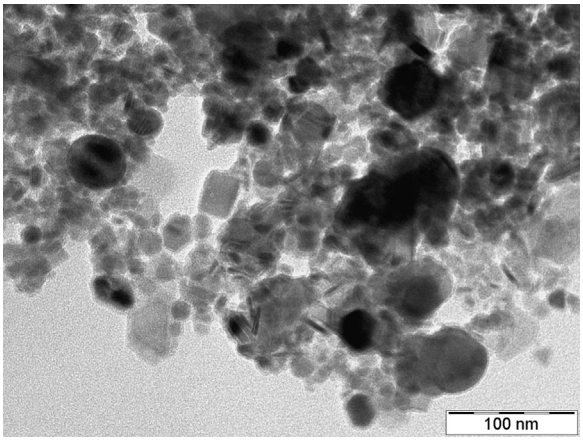

Fig. 6. TEM micrograph of TiO_2+4B.

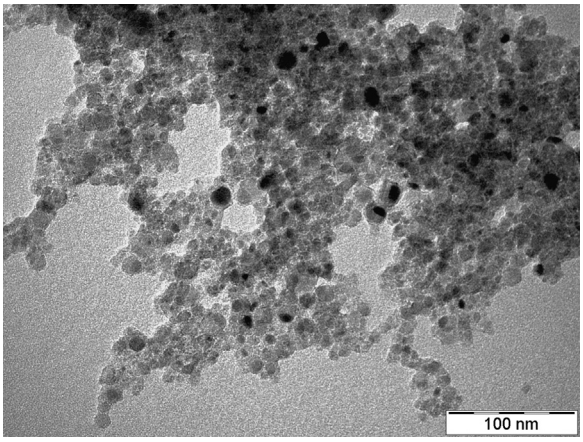

Fig. 7. TEM micrograph of TiO_2+3B+3C.

fully confirm the small particle size derived from SSA data. At least three different contrasts could be distinguished which is in line with the detected different XRD phases. A possible explanation for the restriction of the development of larger TiB_2 crystallites may be the nucleation of B_4C on the surface of TiB_2 crystallites preventing their further growth along the thermal track of the plasma bellow 2500 K. This explanation is confirmed by comparing the FWHM of XRD peaks (Fig. 3). As it can be seen addition of carbon broadened the TiB_2 peaks, which indicate a decrease in crystalline diameters for TiB_2 according to Debye–Scherrer equation.

Finally none of the SEM and TEM micrographs revealed granules significantly larger than 100 nm. This means that all the fed micrometer-sized solid phases evaporated and suffered almost complete transformation during the plasma treatment. In all of the applied conditions, nanosized elementary particles were formed, which created agglomerates of varying sizes in more or less extent.

3.5. Surface analysis

Surface characteristics of the as prepared powder samples were determined by XPS. The results showed the presence of the TiB_2 by the recorded Ti2p and B1s binding energies at 454.5 and 187.5 eV respectively. These data are very close to the reported typical binding energies in titanium borides [29]. The XPS investigations reveal that the surfaces of the obtained powders in all the Runs are severely oxidized. The $Ti2_{p3/2}$ BE at 458.5 eV and the B1s at 193 eV correspond to the oxidized state of titanium and boron, respectively [30]. In detailed analysis of spectra recorded for sample Run 4 we found preferably boron in the carbide state B_4C with B1s at 188.0 eV BE and with C1s at 282.1 eV BE. Large amount (48 at%) of elemental carbon was measured on the surface in agreement with the XRD, and only a very small amount (2 at%) of Ti was detected with $Ti2_{p3/2}$ at 453.1 eV BE, assignable to TiC. Both B and Ti (and also C) was only slightly oxidized in this sample, which could be detected by their chemical shifts (B1s at 193.0 eV, $Ti2_{p3/2}$ at 457.3 eV BE, assignable to Ti_2O_3, detectable also by XRD).

4. Conclusions

Experimental investigation has been performed for continuous synthesis of TiB_2 powder in RF plasma reactor. The particular Runs differed in the type of the feedstock material, all of which comprised of the mixture of micron sized particulates of the reactants. In spite of the short residence time of the reactants in the high temperature plasma the precursors evaporated and reacted to form fine TiB_2 particles. Regardless of the processed precursor system the product powder contained the targeted TiB_2 in the highest amount, albeit its yield significantly differed in the particular Runs. The highest yield of 97% was achieved when nanopowders were prepared by the evaporation of TiB_2 precursor, while TiO_2 reacted with B and C resulted in the lowest yield of 38%. In the rest of investigated reaction routes the yield was around 55%. These values, however, could be increased by optimization of reactants ratio in the precursor. This will be the subject of further investigation with regard to Runs 2 and 3 as the most promising reaction routes. In addition, boron doped titanium Ti(B), TiC and

B_4C phases were also found in smaller amounts as well as oxidized titanium and boron by-products. The obtained phases could be well anticipated on thermodynamic base, even though non-equilibrium phases were also formed due to kinetic reasons. The rapid cooling of the nucleated particles resulted in mainly nano-sized particles with a mean size of less than 100 nm in all Runs. Addition of carbon to the titanium-oxide and boron precursor mixture significantly shifted down the mean particle size to 13 nm. A feasible sequence of the high temperature crystallization was put forward to interpret the restriction of the growth of large TiB_2 crystals in the TiO_2+B+C system, starting with the nucleation of TiB_2 following condensation of B_4C on their surface.

Acknowledgments

The authors also kindly acknowledge the financial support of the National Office for Research and Technology (REG-KM-09-1-2009-0005), Italy-Hungary bilateral mobility grant (TÉT_10-1-2011-0223), and are indebted to the Hungarian Academy of Sciences for the scholarship of two of the authors.

References

[1] S.H. Kang, D.J. Kim, Synthesis of nano-titanium diboride powders by carbothermal reduction, Journal of the European Ceramic Society 27 (2007) 715–718.
[2] C. Subramanian, T.S.R.Ch. Murthy, A.K. Suri, Synthesis and consolidation of titanium diboride, International Journal of Refractory Metals and Hard Materials 25 (2007) 345–350.
[3] R.A. Andrievski, Nanomaterials based on high-melting carbides, nitrides and borides, Russian Chemical Reviews 74 (2005) 1061–1072.
[4] S.E. Kravchenko, V.I. Torbov, S.P. Shilkin, Preparation of titanium diboride nanopowder, Inorganic Materials 46 (2010) 614–616.
[5] N. Chaichana, N. Memongkol, J. Wannasin, S. Niyomwas, Synthesis of nano-sized TiB_2 powder by self-propagating high temperature synthesis, Ciang Mal University Journal of Natural Sciences Special Issue on Nanotechnology 7 (2008) 51–57.
[6] R.L. Axelbaum, D.P. DuFaux, C.A. Frey, K.F. Kelton, S.A. Lawton, L. J. Rosen, S.V. Sastry, Gas-phase combustion synthesis of titanium boride (TiB_2) nanocystallites, Journal of Materials Research 11 (1996) 948–954.
[7] Y. Cheng, M. Shigeta, S. Choi, T. Watanabe, Formation mechanism of titanium boride nanoparticles by RF induction thermal plasma, Chemical Engineering Journal 183 (2012) 483–491.
[8] J. Li, F. Li, K. Hu, Y. Zhou, Formation of TiB_2/TiN/Ti(C_xN_{1-x}) nanocomposite powder via high-energy ball milling and subsequent heat treatment, Journal of Alloys and Compounds 334 (2002) 253–260.
[9] Z. Károly, I. Mohai, S. Klébert, A. Keszler, I.E. Sajó, J. Szépvölgyi, Synthesis of SiC powder by RF plasma technique, Powder Technology 214 (2011) 300–305.
[10] M. Bystrzejewski, Z. Károly, J. Szépvölgyi, W. Kaszuwara, A. Huczko, H. Lange, Continous synthesis of carbon-encapsulated magnetic nanoparticles with a minimum production of amorphous carbon, Carbon 47 (2009) 2040–2048.
[11] J. Szépvölgyi, I. Mohai, Z. Károly, L. Gál, Synthesis of nanosized ceramic powders in a radiofrequency thermal plasma reactor, Journal of the European Ceramic Society 28 (2008) 895–899.
[12] I. Mohai, L. Gál, J. Szépvölgyi, J. Gubicza, Zs. Farkas, Synthesis of nanosized zinc ferrites from liquid precursors in RF thermal plasma reactor, Journal of the European Ceramic Society 27 (2007) 941–945.
[13] J. Szépvölgyi, I. Mohai, J. Gubicza, I. Sáray, RF thermal plasma synthesis of ferrite nanopowders from metallurgical wastes, Key Engineering Materials 264 (2004) 2359–2362.
[14] L. Tong, R.G. Reddy, Synthesis of titanium carbide nano-powders by thermal plasma, Scripta Materialia 52 (2005) 1253–1258.
[15] T. Ishigaki, S.-M. Oh, J.-G. Li, D.-W. Park, Controlling the synthesis of TaC nanopowders by injecting liquid precursor into RF induction plasma, Science and Technology of Advanced Materials 6 (2005) 111–118.
[16] D. Vollath, Plasma synthesis of nanopowders, Journal of Nanoparticle Research 10 (2008) 39–57.
[17] L. Tong, R.G. Reddy, Thermal plasma synthesis of SiC nano-powders/nano-fibers, Materials Research Bulletin 41 (2006) 2303–2310.
[18] P. Fauchais, A. Vardelle, A. Denoirjean, Reactive thermal plasmas: ultrafine particle synthesis and coating deposition, Surface and Coatings Technology 97 (1997) 66–78.
[19] N. Rao, B. Micheel, D. Hansen, C. Fandrey, M. Bench, S. Girshick, J. Heberlein, P. McMurry, Synthesis of nanophase silicon, carbon, and silicon-carbide powders using a plasma expansion process, Journal of Materials Research 10 (1995) 2073–2084.
[20] S.M. Oh, M. Cappelli, D.W. Park, Preparation of nano-sized silicon carbide powder using thermal plasma, Korean Journal of Chemical Engineering 19 (2002) 903–907.
[21] P. Kong, T.T. Huang, E. Pfender, Synthesis of ultrafine silicon-carbide powders in thermal arc plasmas, IEEE Transactions on Plasma Sciences 14 (1986) 357–369.
[22] Y. Leconte, M. Leparoux, X. Portier, N. Herlin-Boime, Controlled synthesis of beta-SiC nanopowders with variable stoichiometry using inductively coupled plasma, Plasma Chemistry and Plasma Processing 28 (2008) 233–248.
[23] M.-J. Chen, C.-Y. Wu, Y.-M. Kuo, H.-Y. Chen, C.-H. Tsai, Preparation of Cu_2O nanowires by thermal oxidation-plasma reduction method, Applied Physics A: Materials Science and Processing 108 (2012) 133–141.
[24] P. Lei, A.M. Boies, S. Calder, S.L. Girshick, Thermal plasma synthesis of superparamagnetic iron oxide nanoparticles, Plasma Chemistry and Plasma Processing 32 (2012) 519–531.
[25] M. Shigeta, T. Watanabe, Multi-component co-condensation model of Ti-based boride/silicide nanoparticle growth in induction thermal plasmas, Thin Solid Films 515 (2007) 4217–4227.
[26] B. Todorovic-Markovic, Z. Markovic, I. Mohai, Z. Károly, L. Gál, K. Föglein, P.T. Szabó, J. Szépvölgyi, Efficient synthesis of fullerenes in RF-thermal plasma reactor, Chemical Physics Letters 378 (2003) 434–439.
[27] J. Szépvölgyi, Z. Markovic, B. Todorovic-Markovic, Z Nikolic, I. Mohai, Z. Fazekas, M. Tóth, É. Kováts, P. Scheier, S. Feil, Effects of precursors and plasma parameters on fullerene synthesis in RF thermal plasma reactor, Plasma Chemistry and Plasma Processing 26 (2006) 597–608.
[28] J.C. Taylor, Computer programs for standardless quantitative analysis of minerals using the full powder diffraction profile, Powder Diffraction 6 (1991) 2–9.
[29] C.D. Wagner, W.M. Riggs, L.E. Davis, J.F. Moulder, Handbook of X-ray Photoelectron Spectroscopy, First ed., Perkin-Elmer Corporation, Eden Prairie, Minnesota, 1979.
[30] I. Bertóti, Nitrogen modified metal oxide surfaces, Catalysis Today 181 (2012) 95–101.
[31] J. Radic-Peric, Formation of gas phase boron and carbon-containing molecular species at high temperatures, Materials Science Forum 555 (2007) 171–176.
[32] FACTSAGE Thermodynamic Equilibrium Software, version 5.0, Center for Research in Computational Thermochemistry of the Ecole Polythechnique at the Université de Montréal and GTT-Technologies, GmbH, Aachen, Germany, 2001.
[33] K. Ostrikov, A.B. Murphy, Plasma-aided nanofabrication: where is the cutting edge?, Journal of Physics D: Applied Physics 40 (2007) 2223–2241
[34] M. Shigeta, A.B. Murphy, Thermal plasmas for nanofabrication, Journal of Physics D: Applied Physics 44 (2011) 174025–174041.
[35] I.E. Sajó, X-ray diffraction quantitative phase analysis of Bayer process solids, in: Proceedings of Travaux ICSOBA, vol. 34, 2008, pp. 46–51.

[36] E. Galvanetto, F.P. Galliano, F. Borgioli, U. Bardi, A. Lavacchi, XRD and XPS study on reactive plasma sprayed titanium-titanium nitride coatings, Thin Solid Films 384 (2001) 223–229.

[37] R.A. Oriani, The Physical and metallurgical aspects of hydrogen in metals, in: Proceedings of ICCF4, Fourth International Conference on Cold Fusion, 1993.

[38] O. Kayacan, S. Sahin, F. Tastan, A study for boronizing process within nonextensive thermostatistics, Mathematical and Computational Applications 15 (2010) 14–24.

[39] M.A. Bejar, E. Moreno, Abrasive wear resistance of boronized carbon and low-alloy steels, Journal of Materials Processing Technology 173 (2006) 352–358.